Computational Mechanics (1993) 12, 164–180

Computational Mechanics

Multiscale finite element method for a locally nonperiodic heterogeneous medium

Jacob Fish and **Amir Wagiman**

Department of Civil Engineering and Scientific Computation Research Center, Rensselaer Polytechnic Institute, Troy, NY 12180, USA

Abstract. A generalization of the mathematical homogenization theory to account for locally nonperiodic solutions is presented. Such nonperiodicity may arise either due to the rapidly varying microstructure (e.g.: graded materials, microcracks) or because the macroscopic solution is not smooth and may have significant variation within a microstructure. In the portion of the problem domain where the material is formed by a spatial repetition of the base cell and the macroscopic solution is smooth, a double scale asymptotic expansion and solution periodicity are assumed, and consequently, mathematical homogenization theory is employed to uncouple the microscopic problem from the global solution. For the rest of the problem domain it is assumed that the periodic solution does not exist (cutouts, cracks, free edges in composites, etc.) and the approximation space is decomposed into macroscopic and microscopic fields. Compatibility between the two regions is explicitly enforced. The proposed method is applied to resolve the structure of the microscopic fields in the single ply composite plates with a centered hole and with a centered crack and in the [0/90]$_s$ laminated plate. Numerical results are compared to the reference solution, an engineering global-local approach, and the direct extraction from the mathematical homogenization method.

1 Introduction

In studying a heterogeneous medium, such as composite materials, one can adopt two different points of view:

(*i*) a microscopic description, where microscopic constituents (with characteristic length l) are considered as a continuous medium, with their own equilibrium, kinematic, constitutive equations and interface conditions with other constituents,

(ii) a macroscopic description, where characteristic microscopic length l is disregarded, and we treat the medium as homogeneous on a much larger (macroscopic) scale, denoted by L, which may represent the dimension of the specimen or a typical wavelength.

Typically, the ratio l/L, denoted here by ε, is very small, and therefore modeling of sizeable problems entirely on the microscale is not realistic. Thus, a double scale asymptotic expansion

$$\boldsymbol{u}(\boldsymbol{x},\boldsymbol{y}) = \boldsymbol{u}^0(\boldsymbol{x},\boldsymbol{y}) + \varepsilon \boldsymbol{u}^1(\boldsymbol{x},\boldsymbol{y}) + \varepsilon^2 \boldsymbol{u}^2(\boldsymbol{x},\boldsymbol{y}) + \cdots \tag{1}$$

where $\boldsymbol{x}$ is a (macroscopic) position vector of the point, $\boldsymbol{y}$ the vector of the stretched (microscopic) coordinates, i.e., $\boldsymbol{y} = \boldsymbol{x}/\varepsilon$, provides a rigorous mathematical framework to simultaneously model phenomena at two different scales. The resulting partial differential equations can be uncoupled into two separate problems (on the micro and macro scales) if, and only if, the following two conditions are satisfied:

(i) microstructure is periodic, i.e., the composite material is locally formed by the spatial repetition of very small microstructures, or unit cells

(ii) $\boldsymbol{u}^k(\boldsymbol{x},\boldsymbol{y})$ terms are periodic in the $\boldsymbol{y}$ variable with the same period as that of the microstructure.

Under these assumptions, the theory known as mathematical homogenization provides a rigorous deduction of macroscopic and microscopic behavior. The fundamentals of this theory can be found, among others, in (Benssousan et al. 1978; Sanchez-Palencia and Zaoui 1985). The engineering counterpart to the homogenization, focusing on defining equivalent thermomechanical properties of a heterogeneous medium, appeared in the engineering literature much earlier. A survey of such activity can be found in (Hashin 1970; Christensen 1979).

Unfortunately, if either material is locally nonperiodic, such as in the case of graded materials, or material is periodic but the solution is not periodic in y variable, such as in the presence of local effects, the use of asymptotic expansion (1) for the purpose of extracting local (microscopic) distribution of stresses and strains, will generally yield poor approximations of the local fields. On the other hand, in practical applications most of the critical behavior occurs in the portion of the problem domain where assumptions (i) and/or (ii) do not hold. This difficulty has been partially resolved for the case of periodic media in the vicinity of free edges (where only assumption (i) holds), by employing an asymptotic expansion of different nature in the boundary layer region and matching the solutions in the outer and inner regions using one of the "matching rules" (Murdock 1991). An excellent discussion of such techniques can be found in (Sanchez-Palencia 1985). Obviously, if either microstructure is nonperiodic, or if the geometry is irregular, a different approach, more suitable for numerical computations is needed.

The primary objective in this paper is to present a consistent mathematical framework to study coupled global-local effects in a heterogeneous medium (which are not necessarily periodic in the sense of assumptions (i) and (ii)). The contents of this paper are as follows: In Sect. 2 the problem domain is decomposed into the periodic and nonperiodic media. In the region where periodicity is assumed, a double scale asymptotic expansion is employed, while in the remaining nonperiodic portion of the problem domain, the displacement field is decomposed into the microscopic and macroscopic fields. Consistent variational framework is employed and continuity of displacement field is explicitly enforced. Section 3 describes the finite element solution procedure to obtain homogenized material properties, macroscopic response, and microscopic information including displacements, stresses and strains. In Sect. 4 we conduct numerical examples to study the structure of the microscopic fields in a single ply composite plate with the hole and with a centered crack and in the $[0/90]_s$ laminated plate employing the present formulation.

2 Problem statement and variational framework

Consider a heterogeneous medium, where the material is formed by the spatial repetition of the base cell on the major portion of the problem domain $\Omega^P \subset \Omega$. On Ω^P we assume that both the microstructure and solution are Y-periodic, i.e., if $\mathbf{Y}(Y_i)$ is a basic period in the stretched coordinate system (see Fig. 1(ii)) and $f(x,y)$ is Y-periodic function on Ω^P, then $f(x,y+k\mathbf{Y}) = f(x,y)$, where k is an integer. To be more precise, we say that in the neighboring points A, B in Fig. 1(ii) homologous by periodicity, the value of the function is almost the same; but in points A, C homologous by periodicity but far away in the x variable, the values of the function are very different.

In the remaining portion of the problem domain $\Omega^L \subset \Omega$ ($\Omega^L \cup \Omega^P = \Omega$ and $\Omega^L \cap \Omega^P = \varnothing$), where the edge effects are dominant or material is not Y-periodic, we make no periodicity assumptions and the solution is assumed to be a function of x only. In order to capture both global and local effects, the displacement field on Ω^L is decomposed into the microscopic and macroscopic

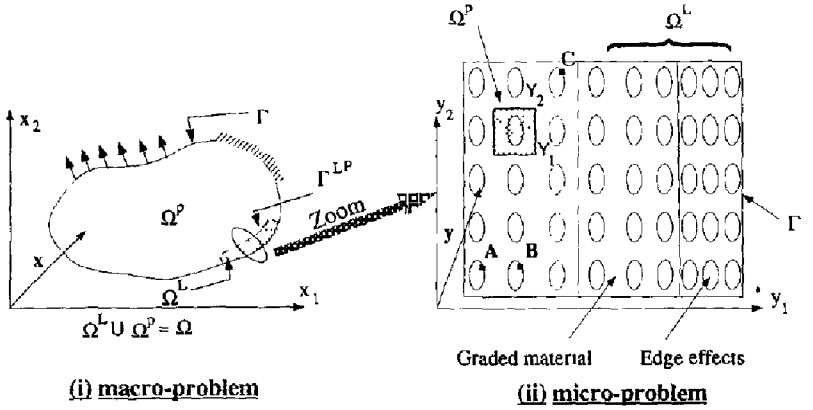

(i) macro-problem (ii) micro-problem

Fig. 1. Two-scale problem definition

fields

$$\boldsymbol{u}(\boldsymbol{x}) = \boldsymbol{u}^P(\boldsymbol{x}) + \boldsymbol{u}^L(\boldsymbol{x}) \quad \text{for} \quad \boldsymbol{x} \in \Omega^L. \tag{2}$$

We start with the formal statement of the strong form of the boundary value problem for linear elastostatics, which states: Find the displacement field $\boldsymbol{u}$ on Ω such that

$$\partial x_j \sigma_{ij} = b_i \quad \text{on} \quad \Omega \qquad \text{(equilibrium equations)} \tag{3a}$$

$$\sigma_{ij} = D_{ijkl}\varepsilon_{kl} \quad \text{on} \quad \Omega \qquad \text{(constitutive equations)} \tag{3b}$$

$$\varepsilon_{kl} = (\partial x_k u_l + \partial x_l u_k)/2 \quad \text{on} \quad \Omega \qquad \text{(kinematical equations)} \tag{3c}$$

$$u_i = g_i \quad \text{on} \quad \Gamma_g \qquad \text{(displacement boundary conditions)} \tag{3d}$$

$$\sigma_{ij} n_j = t_i \quad \text{on} \quad \Gamma_t \qquad \text{(traction boundary conditions)} \tag{3e}$$

where Γ is the boundary of the problem domain Ω, which consists of the prescribed displacement boundary Γ_g and the prescribed traction boundary Γ_t; g_i and t_i are the prescribed displacements and tractions on Γ_g and Γ_t, respectively; b_i are the body forces on Ω; D_{ijkl} is a positive definite constitutive tensor; ∂x_j denotes the partial differentiation with respect to x_j; standard tensorial notation is used with summation over the repeated indexes. Note that in Ω^P, which will be subsequently referred to as a composite domain $\Omega^P(\boldsymbol{x}, \boldsymbol{y})$, the fields $(u_i, \sigma_{ij}, \varepsilon_{kl}, D_{ijkl})$ are functions of $\boldsymbol{x}$ and $\boldsymbol{y}$, while in Ω^L they are functions of $\boldsymbol{x}$ only.

To establish the governing equations on Ω^P in terms of $\boldsymbol{u}^o(\boldsymbol{x}, \boldsymbol{y}), \boldsymbol{u}^1(\boldsymbol{x}, \boldsymbol{y}), \ldots, \boldsymbol{u}^k(\boldsymbol{x}, \boldsymbol{y})$ we insert the asymptotic expansion of $\boldsymbol{u}(\boldsymbol{x}, \boldsymbol{y})$ given in Eq. (1) into the strong form (3) and then identify equal powers of ε. The resulting $o(\varepsilon^{-2})$ and $o(\varepsilon^{-1})$ equations are as follows:

$$o(\varepsilon^{-2})\text{: } \partial y_j(D_{ijkl}\partial y_l u_k^o) = 0, \quad o(\varepsilon^{-1})\text{: } \partial y_j[D_{ijkl}(\partial x_l u_k^o + \partial y_l u_k^1)] = 0 \tag{4a, b}$$

where the chain rule is used to differentiate functions $f(\boldsymbol{x}, \boldsymbol{y} = \boldsymbol{x}/\varepsilon)$

$$\partial x_i[f(\boldsymbol{x}, \boldsymbol{y} = \boldsymbol{x}/\varepsilon)] = \partial x_i f + \partial y_j f \partial x_i y_j = \partial x_i f + \varepsilon^{-1}\partial y_j f. \tag{5}$$

It can be shown (see for example Benssousan 1978, Chap. 1, Sect. 2) that the only Y-periodic function u_k^o that satisfies (4a) is given by

$$u_k^o = u_k^o(\boldsymbol{x}). \tag{6}$$

From Eqs. (6) and (4b), using the same arguments as before, it can be shown (Benssousan 1978) that u_k^1 must be of the form

$$u_k^1 = H_{kij}(\boldsymbol{y})\varepsilon_{ij}^o(\boldsymbol{x}) + \tilde{u}_k^1(\boldsymbol{x}) \tag{7}$$

where

$$\varepsilon_{ij}^o(\boldsymbol{x}) = (\partial x_i u_j^o + \partial x_j u_i^o)/2. \tag{8}$$

The strain field on Ω^P can be found from differentiation of (1) with respect to $\boldsymbol{x}$, which yields

$$\begin{aligned}\varepsilon_{ij}(\boldsymbol{x}, \boldsymbol{y}) = {} & \varepsilon_{ij}^o(\boldsymbol{x}) + 0.5(\partial y_i H_{jkl} + \partial y_j H_{ikl})\varepsilon_{kl}^o(\boldsymbol{x}) \\ & + 0.5\varepsilon(H_{ikl}\partial x_j \varepsilon_{kl}^o + H_{jkl}\partial x_i \varepsilon_{kl}^o + \partial x_i \tilde{u}_j^1 + \partial x_j \tilde{u}_i^1) + o(\varepsilon^2).\end{aligned} \tag{9}$$

For subsequent computations we will consider only $o(1)$ terms, and thus taking the limit of $\varepsilon \to 0$ we obtain the following expressions for the displacement and strain fields:

$$u_i = \begin{cases} u_i^P(\boldsymbol{x}) + u_i^L(\boldsymbol{x}) & \text{for } \boldsymbol{x} \in \Omega^L \quad \text{(10a)} \\ u_i^o(\boldsymbol{x}) & \text{for } \boldsymbol{x} \in \Omega^P \quad \text{(10b)} \end{cases}$$

and

$$\varepsilon_{ij} = \begin{cases} \varepsilon_{ij}^P(\boldsymbol{x}) + \varepsilon_{ij}^L(\boldsymbol{x}) & \text{for } \boldsymbol{x} \in \Omega^L \quad \text{(11a)} \\ \varepsilon_{ij}^o(\boldsymbol{x}) + \Psi_{ijkl}(\boldsymbol{y})\varepsilon_{kl}^o(\boldsymbol{x}) & \text{for } \boldsymbol{x}, \boldsymbol{y} \in \Omega^P \quad \text{(11b)} \end{cases}$$

where

$$\Psi_{ijkl}(\boldsymbol{y}) = 0.5(\partial y_i H_{jkl} + \partial y_j H_{ikl}). \tag{11c}$$

Remark 1: Ψ_{ijkl} possesses minor symmetry (with respect to indices $i \Leftrightarrow j$ and $k \Leftrightarrow l$).

Remark 2: C^0 continuity of the displacement field is enforced by equaling macroscopic and zero order displacement fields

$$u_i^o(\boldsymbol{x}) = u_i^P(\boldsymbol{x}) \quad \text{for } \boldsymbol{x} \in \Omega \tag{12}$$

and constraining the microscopic field $\boldsymbol{u}^L(\boldsymbol{x})$ defined on Ω^L at the interface Γ^{PL} between the two regions

$$\boldsymbol{u}^L(\boldsymbol{x}) = \boldsymbol{0} \quad \text{for } \boldsymbol{x} \in \Gamma^{PL} \tag{13}$$

where Γ^{PL} is defined so that $\Gamma^{PL} \cap \Gamma = \varnothing$.

Remark 3: The inhomogeneous displacement boundary conditions on the boundary of Ω^L are satisfied by the macroscopic field, i.e., $\boldsymbol{u}^P(\boldsymbol{x}) = \boldsymbol{g}(\boldsymbol{x})$ and $\boldsymbol{u}^L(\boldsymbol{x}) = \boldsymbol{0}$ on Γ_g.

Remark 4: Equation (10) shows that the influence of heterogeneity on the displacement field in Ω^P is negligible, while the influence on the strain field is of a comparable order of magnitude to that of the macroscopic strain field. On the other hand, in the region Ω^L, where the local effects are dominant, the influence of heterogeneity on the strain field as well as on the displacement field could be of the same order of magnitude.

We next proceed with the statement of the weak form of the boundary value problem for the linear elastostatics in a locally nonperiodic heterogeneous medium.

Given:

$$\text{(i)}\ \mathscr{U} = \{\boldsymbol{u}(\boldsymbol{x}) | \boldsymbol{u} \in C^0(\Omega),\ \boldsymbol{u} = \boldsymbol{g} \text{ on } \Gamma_g\} \tag{14a}$$

$$\text{(ii)}\ \mathscr{W} = \{\boldsymbol{w}(\boldsymbol{x}) | \boldsymbol{w} \in C^0(\Omega),\ \boldsymbol{w} = \boldsymbol{0} \text{ on } \Gamma_g\} \tag{14b}$$

$$\text{(iii)}\ \mathscr{V} = \{\boldsymbol{v}(\boldsymbol{x}) | \boldsymbol{v} \in C^0(\Omega^L),\ \boldsymbol{v} = \boldsymbol{0} \text{ on } \Gamma_g \cup \Gamma^{PL}\} \tag{14c}$$

$$\text{(iv)}\ \mathscr{H} = \{\boldsymbol{h}(\boldsymbol{y}) | \boldsymbol{h} \in C^0 \text{ (on the unit cell), } \boldsymbol{h} \text{ Y-periodic}\}. \tag{14d}$$

Find $\boldsymbol{u}^o \in \mathscr{U}$, $\boldsymbol{u}^L \in \mathscr{V}$, $H_{kij} \in \mathscr{H}$ and $\boldsymbol{u}$, $\varepsilon(\boldsymbol{u})$ as defined in Eqs. (10, 11), such that for all $\delta \boldsymbol{u}^o \in \mathscr{W}$, $\delta \boldsymbol{u}^L \in \mathscr{V}$, $\delta H_{kij} \in \mathscr{H}$ and the test functions (or variations) defined as

$$\delta u_i = \begin{cases} \delta u_i^P(\boldsymbol{x}) + \delta u_i^L(\boldsymbol{x}) & \text{for } \boldsymbol{x} \in \Omega^L \quad (15a) \\ \delta u_i^o(\boldsymbol{x}) & \text{for } \boldsymbol{x} \in \Omega^P \quad (15b) \end{cases}$$

$$\delta \varepsilon_{ij} = \begin{cases} \delta \varepsilon_{ij}^P(\boldsymbol{x}) + \delta \varepsilon_{ij}^L(\boldsymbol{x}) & \text{for } \boldsymbol{x} \in \Omega^L \quad (16a) \\ \delta \varepsilon_{ij}^o(\boldsymbol{x}) + \Psi_{ijkl}(\boldsymbol{y}) \delta \varepsilon_{kl}^o(\boldsymbol{x}) + \delta \Psi_{ijkl}(\boldsymbol{y}) \varepsilon_{kl}^o(\boldsymbol{x}) & \text{for } \boldsymbol{x}, \boldsymbol{y} \in \Omega^P \quad (16b) \end{cases}$$

$$\delta \Psi_{ijkl}(\boldsymbol{y}) = 0.5\{\delta(\partial y_i H_{jkl}) + \delta(\partial y_j H_{ikl})\} \tag{16c}$$

the following weak form holds

$$\int_{\Omega^P(\boldsymbol{x},\boldsymbol{y})} \delta[\varepsilon_{ij}^o(\boldsymbol{x}) + \Psi_{ijst}(\boldsymbol{y}) \varepsilon_{st}^o(\boldsymbol{x})] D_{ijkl}(\boldsymbol{x},\boldsymbol{y}) [\varepsilon_{kl}^o(\boldsymbol{x}) + \Psi_{klmn}(\boldsymbol{y}) \varepsilon_{mn}^o(\boldsymbol{x})] d\Omega$$
$$+ \int_{\Omega^L} [\delta \varepsilon_{ij}^o(\boldsymbol{x}) + \delta \varepsilon_{ij}^L(\boldsymbol{x})] D_{ijkl}(\boldsymbol{x}) [\varepsilon_{kl}^o(\boldsymbol{x}) + \varepsilon_{kl}^L(\boldsymbol{x})] d\Omega - \int_{\Omega} \delta u_i^o(\boldsymbol{x}) b_i(\boldsymbol{x}) d\Gamma$$
$$- \int_{\Gamma} \delta u_i^o(\boldsymbol{x}) b_i(\boldsymbol{x}) d\Gamma - \int_{\Gamma \cap \Omega^L} \delta u_i^L(\boldsymbol{x}) t_i(\boldsymbol{x}) d\Gamma - \int_{\Omega^L} \delta u_i^L(\boldsymbol{x}) b_i(\boldsymbol{x}) d\Gamma = 0. \tag{17}$$

In order to integrate expressions of the form $f(\boldsymbol{x},\boldsymbol{y})$ over the composite problem domain, $\Omega^P(\boldsymbol{x},\boldsymbol{y})$, we denote that

$$\lim_{\varepsilon \to 0} \int_{\Omega(\boldsymbol{x},\boldsymbol{y})} f(\boldsymbol{x},\boldsymbol{y}) d\Omega \Rightarrow \frac{1}{|Y|} \int_{\Omega(\boldsymbol{x})} \int_{Y} f(\boldsymbol{x},\boldsymbol{y}) dY\, d\Omega \tag{18}$$

where $|Y|$ stands for the volume (or the area in two dimensions) of the unit cell. The above integration scheme can be interpreted as an averaging of an oscillating function in the infinitesimal domain and then subsequent integration of the resulting smooth function over the entire domain. Applying (18) to the first term in (17) yields the following

$$\int_{\Omega} \delta\varepsilon^o_{ij}(x)\tilde{D}_{ijkl}(x)\varepsilon^o_{kl}(x)d\Omega + \int_{\Omega^L} \delta\varepsilon^o_{ij}(x)[D_{ijkl}(x)-\tilde{D}_{ijkl}(x)]\varepsilon^o_{kl}(x)d\Omega + \int_{\Omega^L} \delta\varepsilon^o_{ij}(x)D_{ijkl}(x)\varepsilon^L_{kl}(x)d\Omega$$
$$+ \int_{\Omega^L} \delta\varepsilon^L_{ij}(x)D_{ijkl}(x)\varepsilon^o_{kl}(x)d\Omega + \int_{\Omega^L} \delta\varepsilon^L_{ij}(x)D_{ijkl}(x)\varepsilon^L_{kl}(x)d\Omega - \int_{\Gamma\cap\Omega^L} \delta u^L_i(x)t_i(x)d\Gamma$$
$$- \int_{\Omega^L} \delta u^L_i(x)b_i(x)d\Gamma - \int_{\Omega} \delta u^o_i(x)b_i(x)d\Gamma - \int_{\Gamma} \delta u^o_i(x)t_i(x)d\Gamma + \int_{\Omega^P(x)} \tilde{G}_{ijkl}(x)\varepsilon^o_{ij}(x)\varepsilon^o_{kl}(x)d\Omega = 0 \quad (19)$$

where

$$\tilde{D}_{ijkl} = \frac{1}{|Y|}\int_Y [\delta_{im}\delta_{jn} + \Psi_{mnij}(y)]D_{mnst}(x,y)[\delta_{ks}\delta_{lt} + \Psi_{stkl}(y)]dY \quad (20)$$

$$\tilde{G}_{ijkl} = \frac{1}{|Y|}\int_Y \delta\Psi_{mnij}(y)D_{mnst}(x,y)[\delta_{ks}\delta_{lt} + \Psi_{stkl}(y)]dY. \quad (21)$$

Remark 5: $\tilde{D}_{ijkl}$ is termed as a homogenized constitutive tensor. It can be seen from (21) that it is symmetric and positive definite if the material properties of microconstituents are symmetric and positive definite.

3 Finite element analysis for the locally nonperiodic heterogeneous medium

In this section we describe a finite element solution procedure to obtain homogenized material properties in Ω^P, macroscopic response on Ω, and microscopic information (displacements, stresses and strains) in both Ω^P and Ω^L.

To construct the finite approximation $\mathscr{U}^F, \mathscr{W}^F, \mathscr{V}^F$ of the spaces $\mathscr{U}, \mathscr{W}, \mathscr{V}$, respectively, we subdivide the global problem domain Ω and the local problem domain $\Omega^L \subset \Omega$ into the global and local element subdomains, such that $\bigcup\Omega^o_e = \Omega$ and $\bigcup\Omega^L_e = \Omega^L$, respectively, which are then interpolated using hierarchical basis functions

$$u^o_i = N^o_{iA}d^o_A \quad \delta u^o_i = N^o_{iA}\delta d^o_A, \qquad u^L_i = N^L_{iA}d^L_A \quad \delta u^L_i = N^L_{iA}\delta d^L_A \quad (22a, b)$$

where the upper case subscripts indicate degrees-of-freedom. The displacement field $\boldsymbol{u}(x)$ in the problem domain $\Omega^L \subset \Omega$ is obtained by adding the contributions from the global (macro) and local (micro) finite element meshes. The boundaries of the elements in the two meshes do not have to coincide. The C^o continuity at the interface between the macro and micro meshes Γ^{PL} is imposed by constraining the degrees-of-freedom at the interface Γ^{PL}

$$d^L_A|_{\Gamma^{PL}} = 0. \quad (23)$$

For more details on the various mesh superposition techniques see (Fish et al. 1992, 1993).

In a similar fashion we construct the finite element approximation $\mathscr{H}^F$ of the space $\mathscr{H}$ in the unit cell Y using hierarchical basis

$$H_{ijk} = N^P_{iA}d^P_{jkA} \quad \delta H_{ijk} = N^P_{iA}\delta d^P_{jkA}. \quad (24)$$

The hierarchical shape functions $(\mathbf{N}^o, \mathbf{N}^P, \mathbf{N}^L)$ for a quadrilateral element can be obtained by a tensor product of one-dimensional spectral interpolants $H_J(s)H_I(t)$, which can be defined as integrals of Legandre polynomials, where $s\in[-1,1]$ and $t\in[-1,1]$ are parametric coordinates. The resulting two-dimensional shape functions and their corresponding degrees-of-freedom are termed as nodal ($I, J \leqq 2$), side ($I \leqq 2$, $J > 2$ and $J \leqq 2$, $I > 2$) and internal ($I, J > 2$).

The symmetric gradient fields corresponding to Eqs. (22) and (24) are given by

$$\varepsilon^o_{ij} = 0.5(\partial x_j N^o_{iA} + \partial x_i N^o_{jA}) d^o_A = B^o_{ijA} d^o_A \qquad \delta\varepsilon^o_{ij} = B^o_{ijA}\delta d^o_A \tag{25a}$$

$$\varepsilon^L_{ij} = 0.5(\partial x_j N^L_{iA} + \partial x_i N^L_{jA}) d^L_A = B^L_{ijA} d^L_A \qquad \delta\varepsilon^L_{ij} = B^L_{ijA}\delta d^L_A \tag{25b}$$

$$\Psi_{mijk} = 0.5(\partial y_m N^P_{iA} + \partial y_i N^P_{mA}) d^P_{jkA} = B^P_{miA} d^P_{jkA} \quad \delta\Psi_{mijk} = B^P_{miA}\delta d^P_{jkA}. \tag{25c}$$

Discrete equilibrium equations are obtained by substituting interpolants (22, 24, 25) into the weak form (19–21) and requiring arbitrariness of variations for the following three cases:

(i) $\delta d^o_A = \delta d^L_A = 0$ and $\forall d^P_{jkA} \neq 0$ **Y** periodic
(ii) $\delta d^P_{jkA} = \delta d^L_A = 0$ and $\forall d^o_A \neq 0$
(iii) $\delta d^P_{jkA} = \delta d^o_A = 0$ and $\forall d^L_A \neq 0$.

Condition (i) leads to a unit cell problem in Y applicable only in the portion of the problem domain $\Omega^P \subset \Omega$, while conditions (ii) and (iii) provide a macroscopic response coupled with local effects on $\Omega^L \subset \Omega$. The structure of the resulting system of equations is summarized below:

$$\begin{pmatrix} K^O_{AD} & K^C_{AE} & 0 \\ K^C_{BD} & K^L_{BE} & 0 \\ 0 & 0 & K^P_{CF} \end{pmatrix} \begin{pmatrix} d^o_D \\ d^L_E \\ d^P_{ijF} \end{pmatrix} = \begin{pmatrix} f^o_A \\ f^L_B \\ f^P_{ijC} \end{pmatrix} \tag{26a}$$

$$K^O_{AD} = \int_\Omega B^o_{ijA}\tilde{D}_{ijkl}B^o_{klD}\,d\Omega + \Delta K^O_{AD}, \quad \Delta K^O_{AD} = \int_\Omega B^o_{ijA}(D_{ijkl} - \tilde{D}_{ijkl})B^o_{klD}\,d\Omega \tag{26b, c}$$

$$K^C_{AE} = \int_{\Omega^L} B^o_{ijA} D_{ijkl} B^L_{klE}\,d\Omega, \quad K^L_{BE} = \int_{\Omega^L} B^L_{ijB} D_{ijkl} B^L_{klE}\,d\Omega \tag{26d, e}$$

$$K^P_{CF} = \int_Y B^P_{ijC} D_{ijkl} B^P_{klF}\,dY + \Delta K^P_{CF}, \quad f^o_A = \int_{\Gamma_t} N^o_{iA} t_i\,d\Gamma + \int_\Omega N^o_{iA} b_i\,d\Omega \tag{26f, g}$$

$$f^L_B = \int_{\Gamma_t} N^L_{iB} t_i\,d\Gamma + \int_{\Omega^L} N^L_{iB} b_i\,d\Omega, \quad f^P_{ijC} = -\int_Y B^P_{klC} D_{ijkl}\,dY. \tag{26h, i}$$

Remark 6: Periodicity of boundary conditions in a rectangular geometry of a unit cell implies that the micro-displacement field up to the rigid body motion $\boldsymbol{H}(y)$, the micro-strain field $\Psi(y)$ and the micro-stress field $\boldsymbol{D}(y)\Psi(y)$ are equal on the opposite sides of the unit cell, while the microtractions $\boldsymbol{D}(y)\Psi(y)\mathbf{n}(y)$ are equal and opposite. It is convenient to implement this type of boundary conditions in the existing finite element architecture by connecting pairs of opposite nodes with rigid springs. The stiffness matrix of a rigid spring element connecting a pair of opposite nodes is given by

$$\Delta\mathbf{K}^p_e = p\begin{bmatrix} 1 & -1 \\ -1 & 1 \end{bmatrix} \quad \text{for} \quad p \gg 1 \tag{27}$$

and the assembled stiffness matrix corresponding to all rigid links is denoted by $\Delta\mathbf{K}^P$ (see Eq. 26f). Let $\boldsymbol{d}^p_1$ and $\boldsymbol{d}^p_2$ be the vectors representing degrees-of-freedom on the opposite sides of the unit cell, i.e., $\boldsymbol{d}^p_1 = \boldsymbol{d}^p_2$ and let $\boldsymbol{d}^p_3$ be the internal degrees-of-freedom in the unit cell. Then the partitioned system of equations in the unit cell is given by

$$\begin{pmatrix} \mathbf{K}^p_{11} + \Delta\mathbf{k}^p & \mathbf{K}^p_{12} - \Delta\mathbf{k}^p & \mathbf{K}^p_{13} \\ \mathbf{K}^p_{12} - \Delta\mathbf{k}^p & \mathbf{K}^p_{22} + \Delta\mathbf{k}^p & \mathbf{K}^p_{23} \\ \mathbf{K}^p_{13} & \mathbf{K}^p_{23} & \mathbf{K}^p_{33} \end{pmatrix} \begin{pmatrix} \boldsymbol{d}^p_1 \\ \boldsymbol{d}^p_2 \\ \boldsymbol{d}^p_3 \end{pmatrix} = \begin{pmatrix} \boldsymbol{f}^p_1 \\ \boldsymbol{f}^p_2 \\ \boldsymbol{f}^p_3 \end{pmatrix} \tag{28a}$$

where $\Delta\mathbf{k}^p$ is a sub-block of $\Delta\mathbf{K}^P$. Both, the rigid springs and the $\boldsymbol{d}^p_2$ can be eliminated by adding the first two rows and columns in Eq. (28a), which yields the following system of equations for the unit cell problem

$$\begin{pmatrix} \mathbf{K}^p_{11} + 2\mathbf{K}^p_{12} + \mathbf{K}^p_{22} & \mathbf{K}^p_{13} + \mathbf{K}^p_{23} \\ \mathbf{K}^p_{13} + \mathbf{K}^p_{23} & \mathbf{K}^p_{33} \end{pmatrix} \begin{pmatrix} \boldsymbol{d}^p_1 \\ \boldsymbol{d}^p_3 \end{pmatrix} = \begin{pmatrix} \boldsymbol{f}^p_1 + \boldsymbol{f}^p_2 \\ \boldsymbol{f}^p_3 \end{pmatrix}. \tag{28b}$$

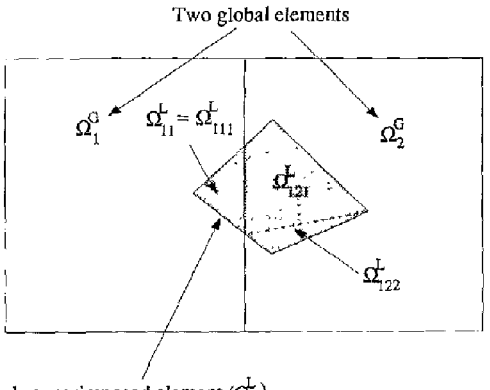

Fig. 2. Numerical integration scheme

Remark 7: Equation (25) shows that as a result of the periodicity assumption in Ω^P the micromechanical problem is completely uncoupled from macromechanical problem. The unknown coefficients $\boldsymbol{d}^P$ are evaluated by solving the micromechanical problem in the unit cell Y for various combinations of indices i and j. Note that the stiffness matrix $\mathbf{K}^P$ is formed and factorized only once and the finite element model in the unit cell is solved for six (three for two dimensional problems) different "loading conditions" (right-hand sides) because of the symmetry in indexes i and j. The homogenized material properties are subsequently determined from the discretization of Eq. (20)

$$\bar{D}_{ijkl} = \frac{1}{|Y|}\int_Y [\delta_{im}\delta_{jn} + B^P_{mnA} d^P_{ijA}] D_{mnst} [\delta_{ks}\delta_{lt} + B^P_{stA} d^P_{klA}] dY \tag{29}$$

and subsequently are used to solve a coupled global-local problem (the first two equations in 26a). For details on the theoretical rates of convergence of homogenized material properties in terms of solution refinement see (Guedes and Kikuchi 1990).

Remark 8: If the solution in the entire problem domain is assumed to be periodic i.e., $\Omega^L \to \varnothing$, then the resulting system of Eqs. (25) degenerates to the classical homogenization problem:

$$\mathbf{K}^o \boldsymbol{d}^o = \boldsymbol{f}^o, \quad \Delta\mathbf{K}^o = 0 \quad \text{and} \quad \mathbf{K}^P \boldsymbol{d}^P = \boldsymbol{f}^P. \tag{30}$$

Remark 9: The microscopic fields (stresses and strains) in both Ω^P and Ω^L can be postprocessed by substituting interpolants (22, 24) into (10, 11). For example, the detailed strain field is given by

$$\varepsilon_{ij} = \begin{cases} B^o_{ijA}(x) d^o_A + B^L_{ijA}(x) d^L_A & \text{for} \quad x \in \Omega^L \quad (31a) \\ [\delta_{ki}\delta_{lj} + B^P_{ijA}(y) d^P_{klA}] B^o_{klB}(x) d^o_B & \text{for} \quad x, y \in \Omega^P. \quad (31b) \end{cases}$$

Remark 10: If local element domains overlap more than a single global element, a special quadrature scheme has been developed in (Fish 1992; Fish and Markolefas 1993; Fish et al. 1993) in order to integrate the coupling stiffness matrix $\mathbf{K}^C$, which contains strain-displacement matrices expressed in the underlying and superimposed element coordinate systems. This integration scheme is briefly summarized here:

(i) Subdivision of superimposed element domains (Ω^L_I) into subelement domains (Ω_{IJ}) defined schematically as (see also Fig. 2):

Loop over all underlying and superimposed elements
If $\Omega^L_I \cap \Omega^G_J \neq \varnothing$ Then $\Omega_{IJ} = \Omega^L_I \cap \Omega^G_J$
End loop

(ii) Subdivision of subelement domains (Ω_{IJ}) into simply shaped domains (Ω_{IJK})—triangles or quadrilaterals in 2D. For elements with straight edges, Ω_{IJ} is a convex polygon, which can be subdivided into convex quadrilaterals (one of which may be collapsed into a triangle) by simply connecting one of the vertices with others as shown in Fig. 2.

(iii) Prior to the execution of the element routines we precompute all the necessary information for integrating the coupling term and store it in the permanent file. In practice, precomputing this information consumes only a small fraction of the total execution time.

For alternative integration schemes see also [10].

Remark 11: Special care must be exercised to avoid the singularity of the stiffness matrix. The singularity or rank deficiency occurs if the local and global meshes have identical deformation modes. The redundant degrees-of-freedom can be constrained either *a priori* in the case of structured superimposed meshes (Kim et al. 1993; Fish et al. 1993), or by eliminating equations with zero pivots which are encountered in the course of the factorization process past the factorization of the base (macro) mesh (Fish et al. 1992, 1993).

4 Numerical examples and discussion

The test problems are divided into two parts. In the first part, we evaluate homogenized material properties using the mathematical homogenization formulation and test the convergence of the equivalent material properties as the finite element mesh of the microstructure is uniformly refined. For comparison purposes, we will also consider the self-consistent method (Hashin 1970; Christensen 1979) for finding the overall material properties of a composite system. In the second part, we test the ability of the proposed superposition method to accurately resolve the microscopic fields of interest in the areas of high stress concentration and compare its performance with the classical method of homogenization and a typical engineering global-local approach described in this section. We consider single-layer composite plates with a centered crack (representing a singular macroscopic solution) and with a centered hole (representing a smooth macroscopic solution) subjected to a uniform tension. Both long and short fiber microstructures are considered. Since our basic mathematical model is two dimensional, fibers are idealized as rectangles.

For the third test case, we analyze a $(0/90)_s$ laminated plate/beam, idealized with two different microstructures corresponding to 0° and 90° layers. Fibers in the 0° layer are idealized as sheets of infinite depth (a plane strain problem), while the fiber cross-section in the 90° layer is idealized by a square.

For all test cases Boron–Aluminium composite system is considered with the following material properties; Boron fiber: Young modulus equal to 400 GPA, and Poisson ratio 0.2; Aluminium matrix: Young modulus equals to 72.5 GPA and Poisson ratio 0.33.

To study the rate of convergence of homogenized material properties we consider a hypothetical checker-board type and long fiber microstructures as shown in Fig. 3. Meshes with 4×4, 6×6, 8×8 and 10×10 elements are used. The results in Fig. 3 show the linear rate of convergence of the equivalent material constants as the finite element mesh is uniformly refined. In the case of long fiber microstructure a very coarse mesh provides almost exact results since the strain field is almost uniform, while with short fiber microstructure a significantly greater refinement is needed to obtain the same level of accuracy.

An engineering approximation technique for finding the overall material properties of a composite system—the self-consistent method—was also employed for comparison. For this purpose, the fiber volume ratios for the long and short fiber microstructures were taken as 0.5 and 0.375, respectively. It should be noted that the formulation of the self-consistent method is based on the assumption that the inclusion (fiber) is a ellipsoidal shape which is embedded in a homogeneous overall medium. The mathematical homogenization formulation, on the other hand, accounts for the precise (idealized) geometry of the microstructure. Differences in the overall moduli found by the self-consistent method and the mathematical homogenization technique are therefore expected. Table 1 compares the results obtained from the self-consistent method and the mathematical homogenization method. The self-consistent method yields slightly higher values of the overall elastic constants compared to those obtained from the mathematical homogenization method.

Numerical results for the Crack, Hole and Beam problems are compared to those obtained from the reference solution, the direct post-processing from the mathematical homogenization

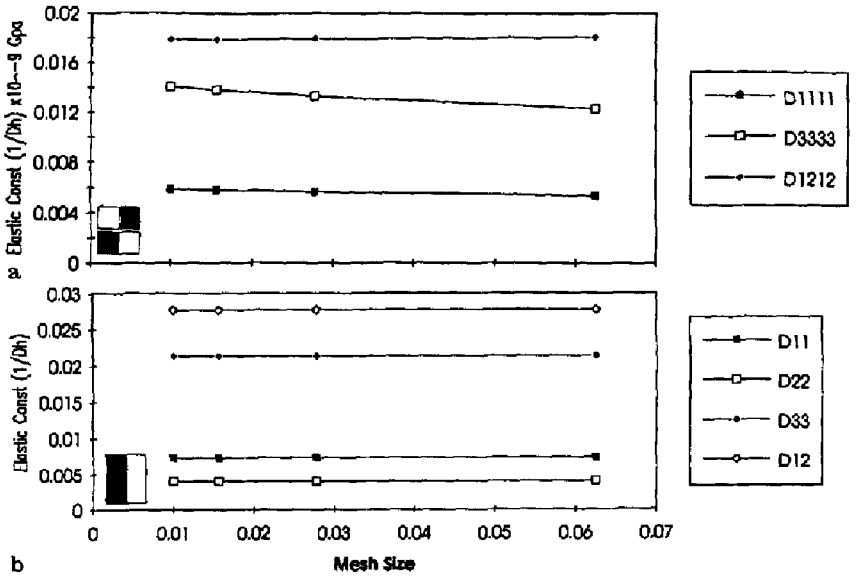

Fig. 3. Convergence of the homogenized material properties for the checker-board and long fiber microstructures

Table 1. Comparison of the self-consistent and mathematical homogenization techniques

	Long fiber model		Short fiber model	
	Mathematical homogenization	Self-consistent	Mathematical homogenization	Self-consistent
D1111	136.147	165.548	122.457	132.491
D2222	245.81	247.575	151.351	205.753
D1212	46.85	64.887	42.112	51.384
D1122	36.076	42.048	36.191	36.926

All values are in Gpa

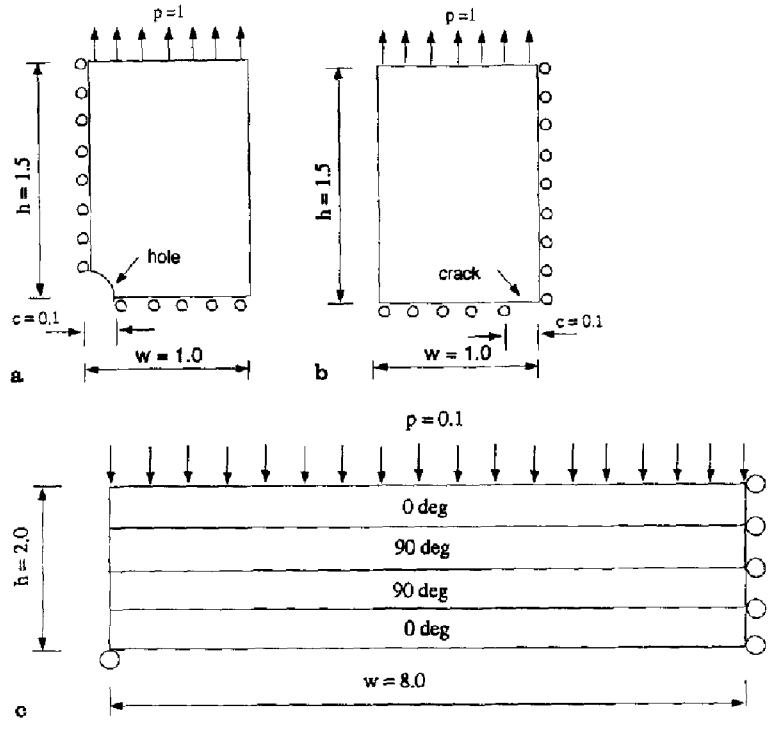

Fig. 4. Geometry and boundary conditions of the test cases

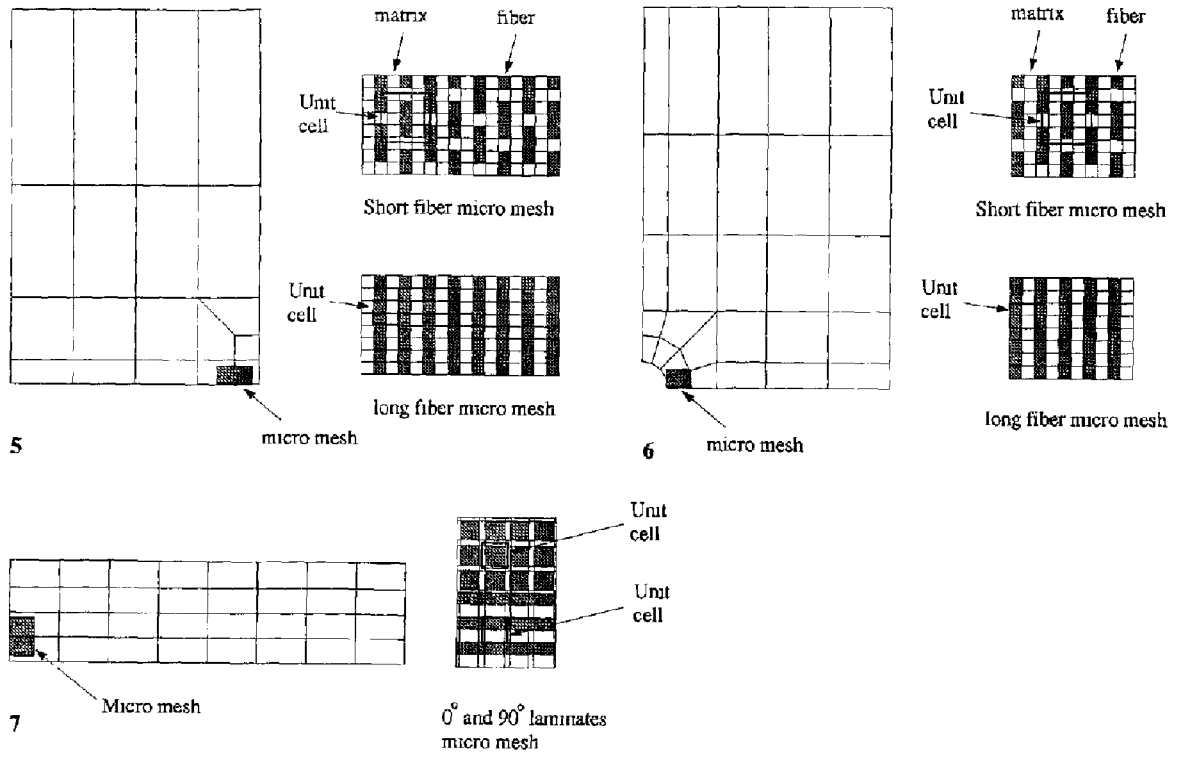

Figs. 5–7. Global (macro) and local (micro) finite element meshes: **5** for the Crack problem, **6** for the Hole problem, **7** for the Beam problem

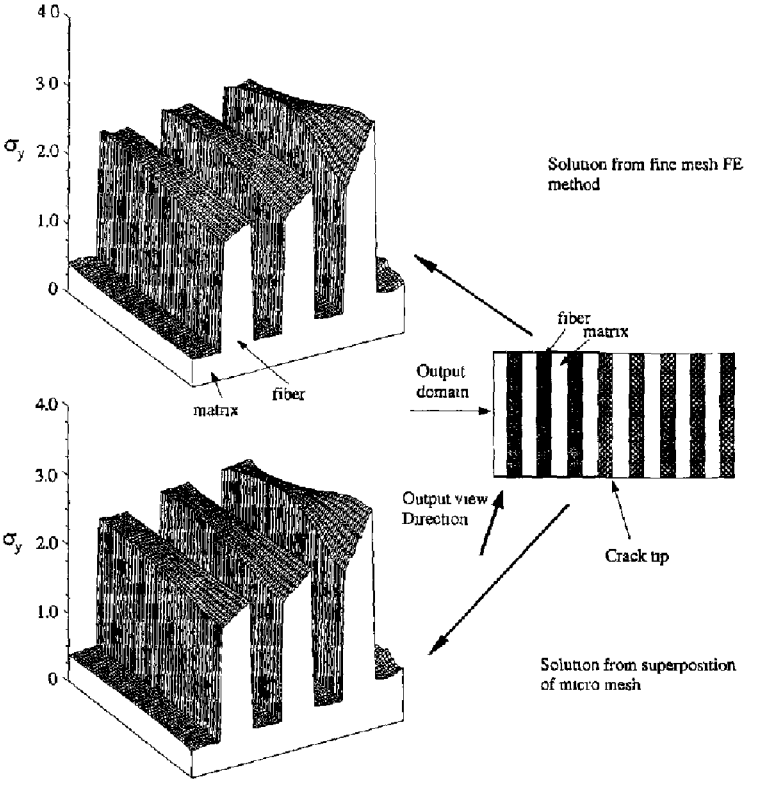

Fig. 8. Crack problem with long fiber microstructure: Surface plots of σ_y in the micro domains obtained using the reference solution and the superposition method

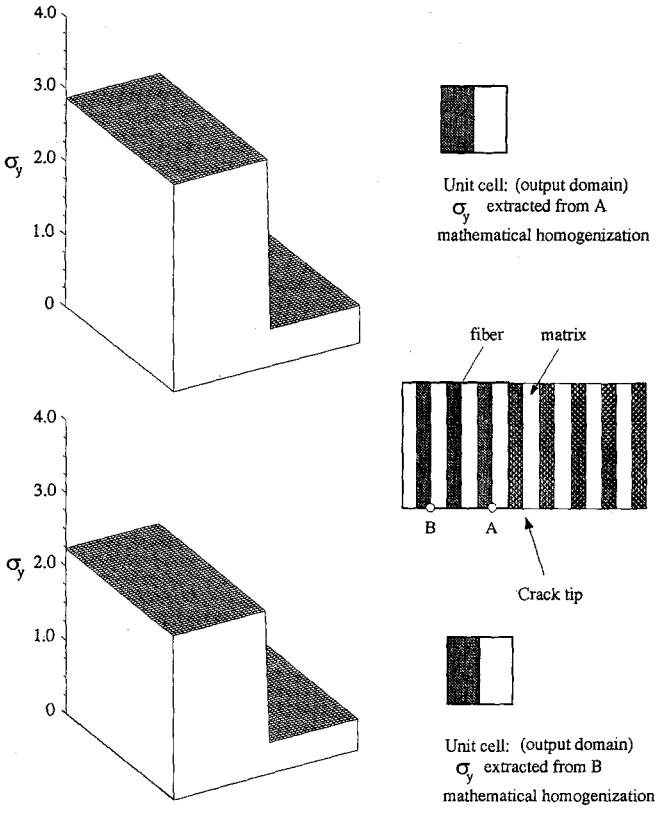

Fig. 9. Crack problem with long fiber microstructure: Surface plots of σ_y obtained from the post processing of the mathematical homogenization method

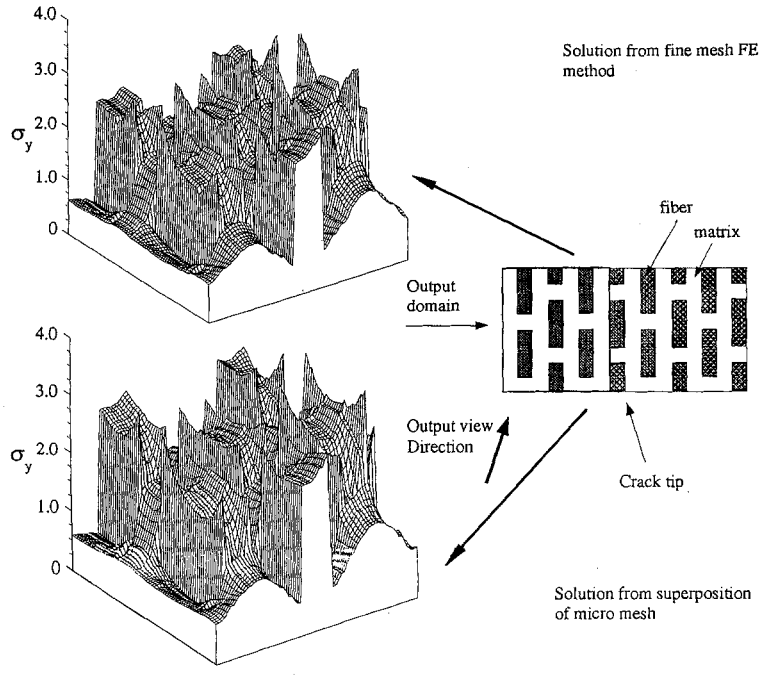

Fig. 10. Crack problem with short fiber microstructure: Surface plots of σ_y in the micro domains obtained using the reference solution and the superposition method

formulation, and the engineering global-local technique. The geometry, loading and boundary conditions for all three problems are given in Fig. 4. For the Crack problem, c is the half length of the crack, w the half width of the plate, and h the half length of the plate; the ratio c/w is chosen to be 0.1. For the Hole problem, c is the radius of the hole, w the half width of the plate, and c/w is taken as 0.1. For the Beam problem, h is the total thickness of the beam and w the half length

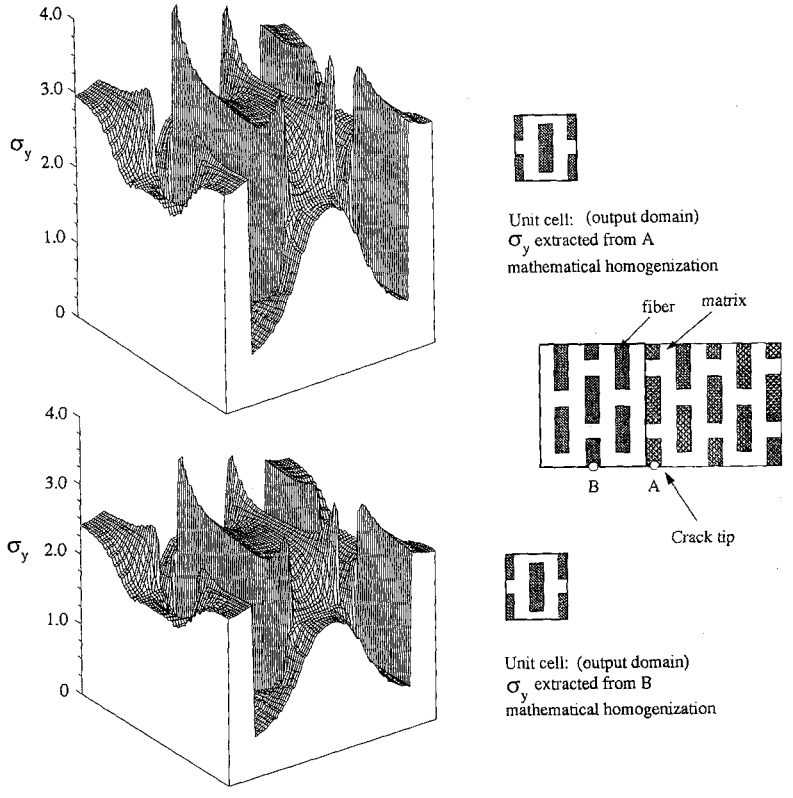

Fig. 11. Crack problem with short fiber microstructure: Surface plots of σ_y obtained from the post processing of the mathematical homogenization method

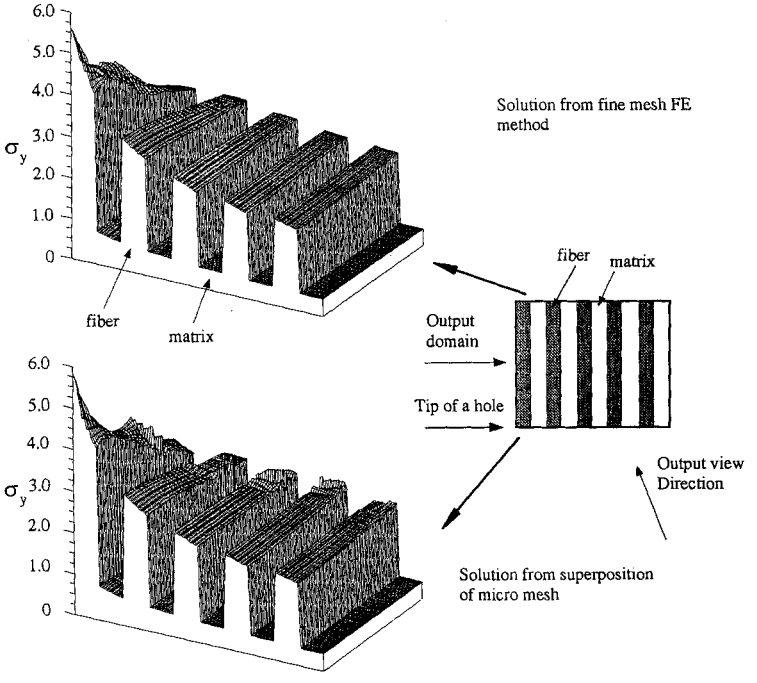

Fig. 12. Hole problem with long fiber microstructure: Surface plots of σ_y in the micro domains obtained using the reference solution and the superposition method

of the beam span; the fiber volume ratio in both layers is taken to be 0.5. For simplicity, the value of the applied traction in the global domain is set to 1.0 for both Crack and Hole problems, while for the Beam problem, the uniform applied traction is taken as 0.1.

The issue of finding the optimal location and the polynomial order for the superimposed meshes is not addressed here. Instead, some experience gained with *p*- and *s*-methods is used here

as a general guideline to construct the global and superimposed meshes. The global and local (micro) finite element meshes for all test cases considered are presented in Figs. 5–7. The topography of the micro meshes is chosen so that it would accurately represent the geometrical features of the microconstituents. For all test cases, the polynomial order of the global and local meshes is taken to be three and four, respectively.

For the reference finite element solution, the mesh is strongly graded towards the high gradient region of interest. Within this region, the finite element mesh is identical to that used in the superposition formulation.

Figures 8–11 show the surface plots of σ_y for the Crack problem as extracted from the reference solution, the superposition method, and the post-processing from the mathematical homogenization formulation for both the long and short fiber microstructures. The solution at the singularity is not included in the plots; the output domain starts from the matrix next to the fiber neighboring the crack tip and extends to the next three fibers (see Figs. 8 and 10). The mathematical homogenization post-processing results are shown at two different locations: one near the high stress gradient region (point A in Figs. 9 and 11) and the other (point B in Figs. 9 and 11) away from the high stress gradient region.

For the long fiber microstructure, it can be seen that in the vicinity of the crack, the superposition method predicts significant variation of the stress field within the fiber itself whereas the mathematical homogenization technique shows constant stress within the fiber and the matrix regardless of the macroscopic location. Away from the high stress gradient region, the solution obtained from the superposition method is almost identical to that obtained from the mathematical homogenization technique.

For the short fiber microstructure, similar trend is observed: The superposition method captures high stress gradients at the crack tip as well as the mild stress concentration at the corners of short fibers. Away from the high gradient region, similar stress distribution is observed with both, the superposition and the mathematical homogenization methods. For both microstructures the results obtained with the superposition method are in good agreement with the reference solution.

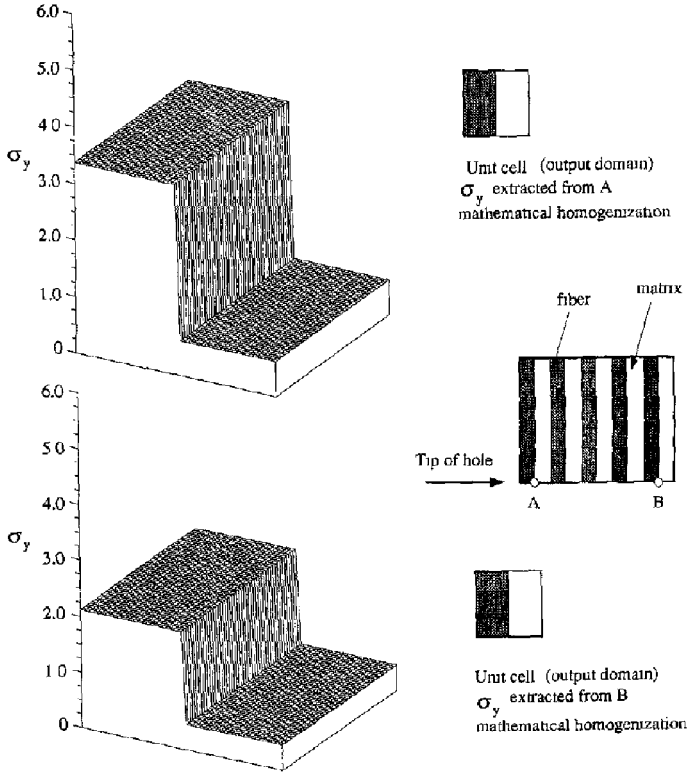

Fig. 13. Hole problem with long fiber microstructure: Surface plots of σ_y obtained from the post processing of the mathematical homogenization method

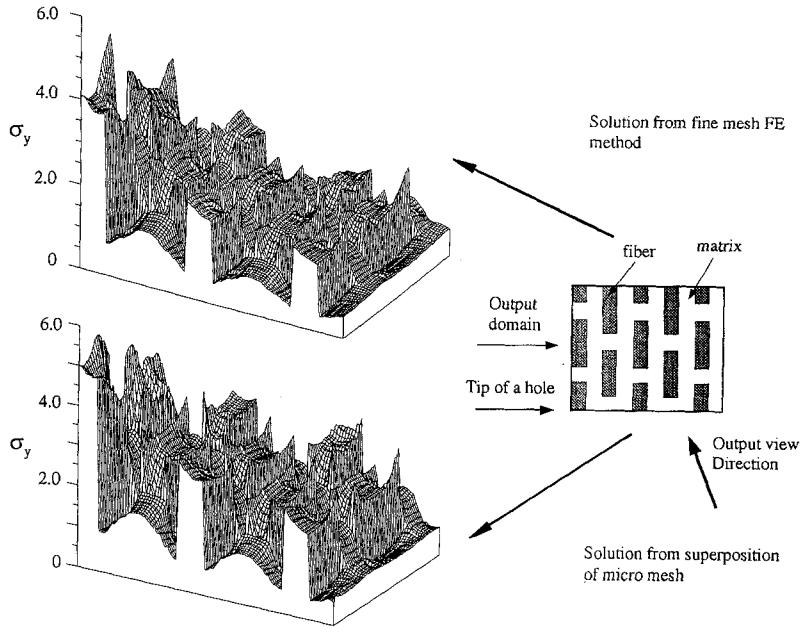

Fig. 14. Hole problem with short fiber microstructure: Surface plots of σ_y in the micro domains obtained using the reference solution and the superposition method

The surface plots of σ_y for the Hole problem are presented in Figs. 12–15. In the long fiber microstructure case, the superposition method yields a maximum stress value of 5.75 near the hole, while the reference solution yields 5.6 and the post-processing from homogenization, 3.4. As in the Crack problem, the superposition method predicts significant stress variation within the fiber itself in the close vicinity of the hole and it is in good agreement with the reference solution. Slight disturbances can be seen (Fig. 12) at the boundary between the two global elements due to the insufficient refinement in the global mesh.

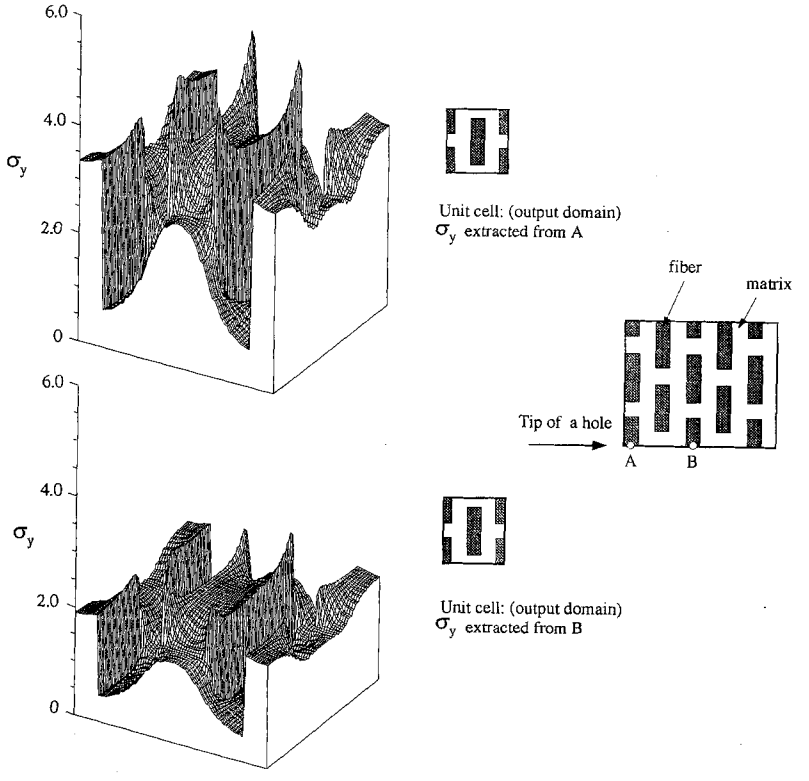

Fig. 15. Hole problem with short fiber microstructure: Surface plots of σ_y obtained from the post processing of the mathematical homogenization method

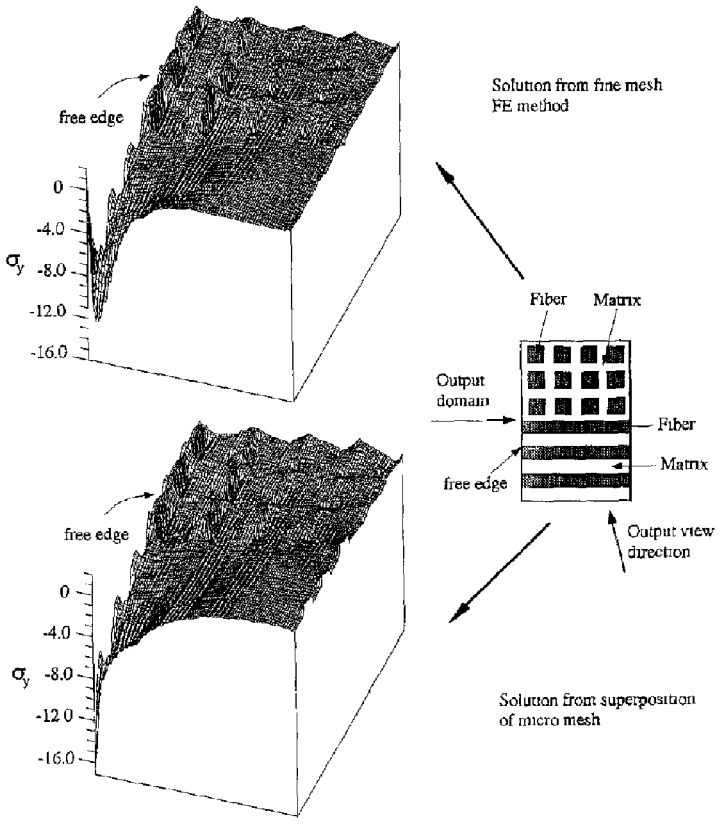

Fig. 16. Beam problem: Surface plots of σ_y in the micro domains obtained from the reference solution and the superposition method

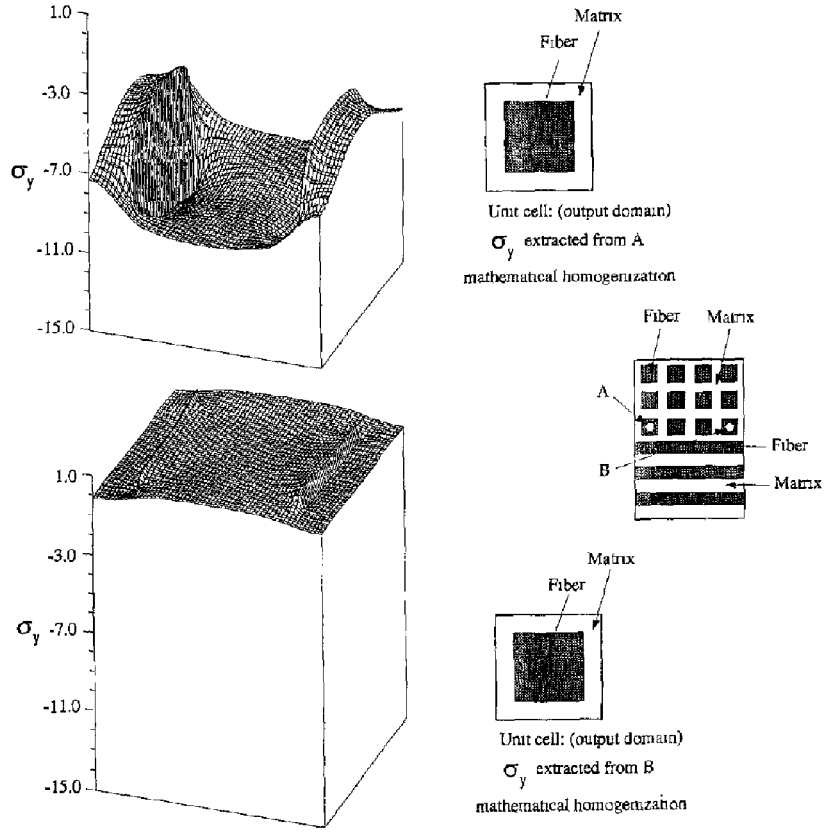

Fig. 17. Beam problem: Surface plots of σ_y obtained from the post processing of the mathematical homogenization method

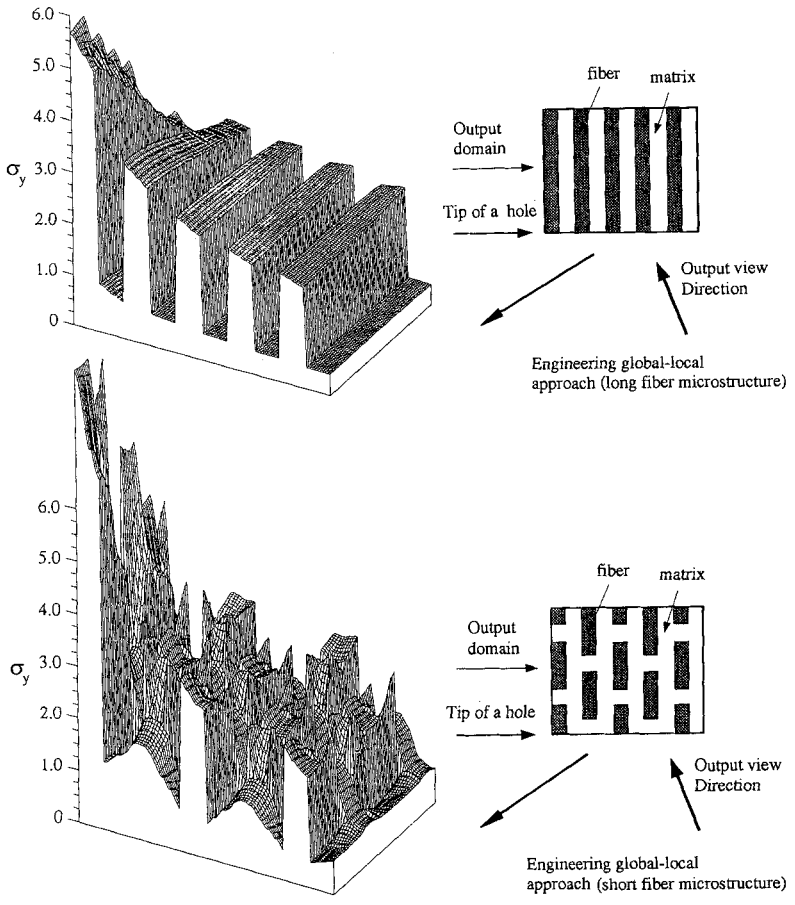

Fig. 18. Uncoupled global-local FE method for the Hole problem: Surface plots of σ_y in the micro domain for the long and short fiber microstructures

For the Beam problem, Figs. 16 and 17 show the surface plots of the peeling stress σ_y within the region where delamination normally initiates, i.e., at the junction of 0/90 interface and the free edge as shown in Fig. 7. Both the reference solution and the superposition method predict significant stress gradients at the junction between the free edge and the fiber-matrix interface mainly due to the two-dimensional idealization of the problem. This is to be expected, since mild stress singularity is present at the interface between any two different materials at the free edge. Figure 17 shows that the peeling stress σ_y obtained from the mathematical homogenization formulation in a 90° layer is in good agreement with the reference solution and the superposition method. However, in a 0° layer the homogenization theory predicts a constant peeling stress field in the entire problem domain and does not sense the presence of the free edge singularity.

The possibility of using a typical engineering global-local approach in order to extract the microscopic fields of interest is also examined. By this technique one solves the global problem first, and then the displacements away from the hot spots are applied as essential boundary conditions on the local domain of interest. This approach has been tested for the Hole problem with both the long and short fiber microstructures. The geometry and the finite element mesh for the local domain have been chosen to be identical to those of the superimposed mesh shown in Fig. 6. σ_y results are given in Fig. 18. It can be seen that for the long fiber case, where the stress distribution is generally smooth within each phase, the overall stress distribution and the maximum stress values are predicted with a reasonable engineering accuracy. On the other hand, for the short fiber case, where the stress oscillations are encountered within each phase, the stress value at the tip of a hole is overestimated by a factor of two, and the quality of the overall stress predictions strongly degrades in the close vicinity of the hole.

One may possibly improve the performance of the uncoupled global-local technique by subjecting a local domain of interest to the boundary conditions extracted from the postprocessing in the unit cell. This will necessitate the postprocessing of the microsolution (displacements or

tractions) on the entire interface between the global and local domains, and thus the practicality of this approach from the engineering standpoint becomes questionable, especially in the three-dimensional case.

Conceptually, the superposition method and the coupled global-local approach, where homogenized material properties are used in the global region and the material properties of microconstituents in the local region, are similar in the sense that the global and local solutions are coupled. Besides from the theoretical differences, there are several key practical issues making the superposition method advantageous.

(i) The superposition method does not require constraint equations or transition zones between the global and local regions. Compatibility between the two regions is explicitly enforced.

(ii) The superposition method is hierarchical in the sense that the global stiffness matrix, representing the overall behavior of the entire model, can be used as a preconditioner, $\mathbf{P}$, to the coupled global-local model. To fix ideas we return to the Hole problem with short fiber microstructure. The condition number (the ratio between the largest and the smallest eigenvalues) of the coupled stiffness matrix (the first two equations in 26a) preconditioned with the Jacobi preconditioner is 2743. On the other hand, the condition number of the preconditioned system with the block diagonal preconditioner ($\Delta\mathbf{K}^o$ neglected to preserve the previous factorization of $\mathbf{K}^O$) defined as

$$\mathbf{P}=\begin{bmatrix}\mathbf{K}^O & \mathbf{0}\\ \mathbf{0} & \mathbf{K}^L\end{bmatrix} \tag{32}$$

is only 222. Furthermore, the solution from the homogenized model is used as an initial guess in the iterative process in solving the coupled problem. More details on the theoretical aspects and application of the preconditioned conjugate gradient and hierarchical multigrid methods in conjunction with the superposition method will appear in reference (Fish et al. 1993).

Acknowledgments

The support of the NASA Langley Research Center under the Grant NAG-1-1356 and National Science Foundation under Research Initiation Award ECS-9003093 are gratefully acknowledged.

References

Benssousan, A.; Lions, J. L.; Papanicoulau, G. (1978): Asymptotic analysis for periodic structures. Amsterdam: North Holland

Christensen, R. M. (1979): Mechanics of composite materials. New York: Wiley

Fish, J.; Markolefas, S. (1992): The *s*-version of the finite element method for multilayer laminates. Intern. J. Numer. Meth. Eng. 33/5, 1081–1105

Fish, J. (1992): Hierarchical modeling of discontinuous fields. Communications in Appl. Numer. Meth. 8, 443–453

Fish, J. (1992): The *s*-version of the finite element method. Comput. & Struct. 43/3, 539–547

Fish, J.; Markolefas, S. (1993): Adaptive *s*-method for linear elastostatics. Comp. Meth. Appl. Mech. Engng. (accepted)

Fish, J.; Fares, N.; Nath, A. (1993): Micromechanical elastic cracktip stresses in a fibrous composite. Intern. J. Fracture (accepted)

Fish, J.; Markolefas, S.; Guttal, R.; Nayak, P. (1993): Progress with the *s*-version of the finite element method. Appl. Numer. Math. (accepted)

Guedes, J. M.; Kikuchi, N. (1990): Preprocessing and postprocessing for materials based on the homogenization method with adaptive finite element methods. Comp. Meth. Appl. Mech. Engng. 83, 143–198

Hashin, Z. (1970): Theory of composite materials. In: Wend, F. W.; Liebowitz, H.; Perrone, N. (eds.) Mechanics of composite materials. Oxford: Pergamon

Kim, Y. H.; Levit, I.; Stanley, G. (1993): A finite element adaptive refinement technique that avoids multipoint constraints and transition zones. J. Appl. Mech. (accepted)

Murdock, J. A. (1991): Perturbations theory and methods. New York: Wiley

Sanchez-Palencia, E.; Zaoui, A. (1985): Homogenization techniques for composite media. Berlin, Heidelberg, New York: Springer

Sanchez-Palencia, E. (1985): Boundary layers and edge effects in composites. Homogenization techniques for composite media. Berlin, Heidelberg, New York: Springer

Communicated by S. N. Atluri, December 15, 1992